III–VI SEMICONDUCTORS

Semiconductors based on compounds of group III and group VI elements are receiving increasing attention worldwide. These elements are found as either constituents or dopants in more traditional semiconducting materials such as group VI (Si, Ge), III–V (GaAs, AlAs, etc.), or II–VI (ZnSe, CdTe, etc.) materials. The III–VI compounds are therefore chemically compatible with the more traditional semiconducting materials, and they exhibit similar (optical) bandgaps and lattice constants (see Fig. 1) The III–VI compounds, on the other hand, have many distinct structural, electronic, and optical properties that are not found in the traditional group VI, III–V, or II–VI materials. This combination of features holds significant promise for the development of semiconducting III–VI compounds as new device materials.

The III–VI semiconductors comprise two principal stoichiometries (1): (a) $A^{III}B^{VI}$ compounds such as GaS, GaSe, and InSe and (b) $A_2^{III}B_3^{VI}$ compounds such as Ga_2S_3, Ga_2Se_3, and In_2Se_3. In addition, $A_2^{III}B^{VI}$ compounds such as Ga_2Se may be possible from the phase diagram (2). Typical crystal structures for the $A^{III}B_{VI}$ and $A_2^{III}B_3^{VI}$ materials are shown in Figs. 2(a) and 2(b), respectively, and some relevant properties of these materials are summarized in Table 1.

The $A^{III}B^{VI}$ compounds present a layered structure, exhibiting weak bonding between separate, covalently bonded B-A-A-B layers (A = Ga, In; B = S, Se, Te; see Fig. 2(a). The

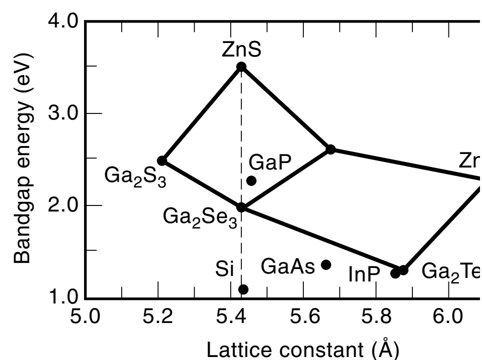

Figure 1. Bandgap versus lattice constant of various III–VI semiconductors.

J. Webster (ed.), *Wiley Encyclopedia of Electrical and Electronics Engineering*. Copyright © 1999 John Wiley & Sons, Inc.

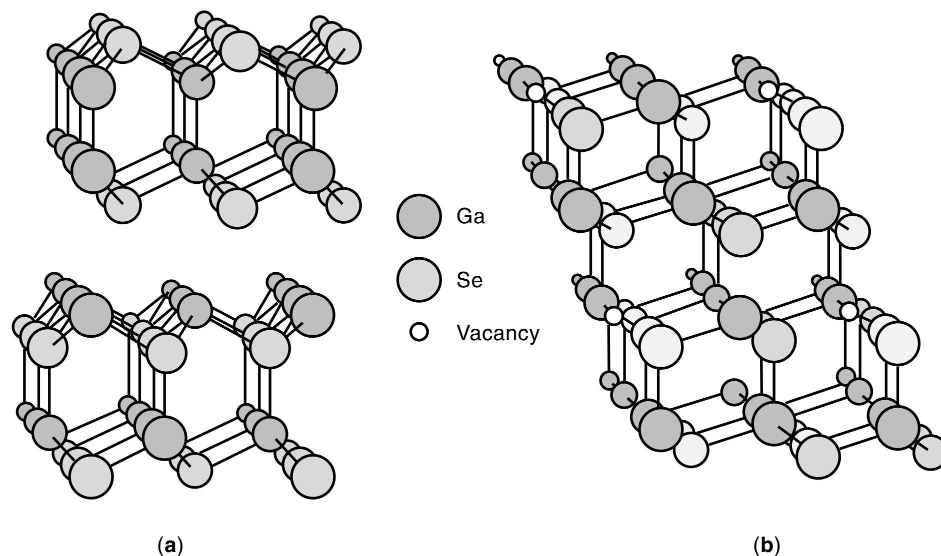

Figure 2. Crystal structure of (a) ϵ-GaSe and (b) β-Ga_2Se_3. Covalent bonds are denoted by lines. Note the layers in GaSe and the vacancies in Ga_2Se_3. The most common polytypes for stacking the GaSe layers are shown in Fig. 3.

interaction between adjacent layers is "van der Waals" type, exhibiting weak bonding between separate, covalently bonded layers; these materials are often referred to as "van der Waals materials." The layered crystal structure results in strong optical and electrical anisotropy (3,4). In addition, the layered $A^{III}B^{VI}$ compounds have attracted much attention because of their high nonlinear optical coefficient in the infrared ranges, making them candidates for second harmonic generation (SHG) materials (3,5–7). This interest led to vital activity to fabricate bulk single crystals of GaSe and InSe, and many optical and electrical properties were investigated in the 1970s and 1980s. Fernelius (8) has extensively reviewed the

Table 1. Properties of Selected $A^{III}B^{VI}$ and $A_2^{III}B_3^{VI}$ Materials (80)

Material	Structure	a_0 (Å)	c_0 (Å)	ρ (g/cm^3)	E_G (direct) (eV)	E_G (indirect) (eV)	ϵ(0)	ϵ(∞)
β-GaS	Hexagonal layers (A-A′-A . . .)	3.587	15.49	3.86	3.0	2.6	5.9 (II) 10.0 (P)	5.3 (II) 6.7 (P)
ϵ-GaSe	Hexagonal layers (A-B-A . . .)	3.755	15.95	5.03	2.1	2.1	6.18 (II) 10.6 (P)	5.76 (II) 7.44 (P)
γ-GaSe	Hexagonal layers (A-B-C-A . . .)	3.755	23.92					
ϵ-GaTe	Hexagonal layers (A-B-C-A . . .)	4.06	16.90					
GaTe	Monoclinic tilted layers	17.44 10.46	4.077	5.44	1.7		10.6 (II) 9.66 (P)	7.29 (II) 6.97 (P)
ϵ-InSe	Hexagonal layers (A-B-A . . .)	4.00	16.70	5.55	1.2	1.3	5.4 (II) 8.6 (P)	4.9 (II) 6.2 (P)
α-Al_2S_3	Wurtzite (ordered vacancy)	6.423	17.83	2.32				
Al_2Se_3	Wurtzite (disordered vacancy)	3.89	6.30	3.91				
α-Ga_2S_3	Wurtzite (ordered vacancy)	11.09 9.578	6.395		3.4			
β-Ga_2S_3	Wurtzite (disordered vacancy)	3.678	6.016	3.65	2.5			
γ-Ga_2S_3	Zincblende (disordered vacancy)	5.418		3.63			7.5	5.8
β-Ga_2Se_3	Zincblende (ordered vacancy)	23.235	10.83	4.91	1.8–2.1	2.0		
Ga_2Te_3	Zincblende (disordered vacancy)	5.874		5.57	1.2			
β-In_2S_3	Spinel (ordered defect)	7.618	32.33	4.61	2.0	1.1		
In_2Se_3	Varied (layered Se-In-Se-In)				1.16	1.0	16.7 (II)	9.5 (II)
β-In_2Te_3	Zincblende (disordered vacancy)	6.163		5.73	1.0		16	11.6

physical properties of GaSe single crystals from around 600 articles published prior to 1992.

Compounds of stoichiometry $A_2^{III}B_3^{VI}$ are common, since the valences for the group III and VI elements are +3 and −2, respectively. Chalcogenide-based $A_2^{III}B_3^{VI}$ materials, however, are considerably different from oxides like Al_2O_3 and B_2O_3. Structurally they form a defected zincblende or wurtzite structure, with one-third of the cation sites empty; thus $A_2^{III}B_3^{VI}$ can be doped to a higher level than other conventional tetrahedral levels of vacancies. This causes an anomaly in the electronic state of impurities and electrical neutrality accommodated by these defects (9), resulting in the fact that the semiconducting properties remain unchanged even at a significant impurity concentration. The crystal structures of these materials also explain the high stability for radiation with regard to a number of parameters, such as optical constants in the infrared (IR) region (10).

Interest in $A_2^{III}B_3^{VI}$ materials, in particular Ga_2Se_3, stems from the interfacial reaction involved in II–VI or III–V heteroepitaxy; but the information of Ga_2Se_3 during the initial stage of the ZnSe/GaAs interface formation was found to be a severe obstacle, leading to a disruption of the interface (11–13). However, Ga_2Se_3 is a potentially useful material in its own right. Ga_2Se_3 serves as a good candidate for the passivation of the GaAs(100) surface (14,15) and has strong potential for use in optoelectronic devices. Recent work has shown the bandgap to be 2.6 eV (in contrast to earlier measurements of ≈2.0 eV) (16), leading to the potential use for operation at the short wavelength (500–400 nm) end of the visible spectrum. Furthermore, large absorption anisotropy ($\Delta\alpha > 10^4$ cm^{-1}) has been observed in vacancy-ordered Ga_2Se_3 (17). The close lattice matching of zincblende Ga_2Se_3 to materials like Si, GaP and ZnS suggests its use in heterostructures. In particular, ZnS-Ga_2Se_3 superlattices growth on GaP are attractive for tunable-color LEDs because of large difference in bandgap energies (16). Superlattices of Ga_2S_3–Ga_2Se_3 have also been proposed for blue lights emitting devices (LEDs). The lower ionicity of these materials may also facilitate easier *p*-type doping than is the case with II–VI compound semiconductors (18).

Despite these intriguing possibilities, knowledge about the properties of III–VI materials is still severely limited by the lack of good-quality single-crystal materials. In addition, bulk III–VI semiconductors are quite difficult to work with due to their poor mechanical and thermal properties. However, these problems may be overcome through the use of thin films. Heteroepitaxial III–VI films are of particular importance both as possible novel materials for electronic and/or optoelectronic devices and as prototypes addressing the basic physical chemistry governing heteroepitaxy of dissimilar materials. This chapter deals with some of the important progress that has been made in the past decade, mainly focusing on the thin-film growth of III–VI compound semiconductors.

CRYSTAL, CHEMICAL BONDING, AND ELECTRONIC STRUCTURE

$A^{III}B^{VI}$ Compounds

In the layered $A^{III}B^{VI}$ compounds, each layer is structurally identical and is composed of single planes of group VI atoms on either side of a double plane of group III atoms [see Fig. 2(a)]. The layered structure can be regarded as a spontaneous superlattice formed by stacking four monoatomic sheets in a B-A-A-B sequence. The vertical alignment of the top and bottom anion layers [see Fig. 2(a)] is characteristic of trigonal prismatic symmetry. Different stackings of these covalently bonded layers result in several polytypes. The polytypes, β, ϵ, and γ, differ by the stacking of the layers regularly in the three relative positions permitted by the layered structure as shown in Fig. 3 (19). In the β-polytype, adjacent layers in the hexagonal unit cell are rotated by 60° with respect to each other and translated by $\sqrt{3}a/c$ in the hexagonal [210] direction, where a is the hexagonal unit-cell dimension. The space group is $D_{6h}^4 - P6_3/mmc$. For the ϵ- and γ-polytypes, no relative rotation of the layer is required, but only a translation. The ϵ- and γ-polytypes belong to space groups $D_{3h}^1 - P\overline{6}\ m2$ and $C_{3v}^5 - R3m$, respectively. The β- and ϵ-polytypes possess no inversion center between the layers, whereas the γ-polytype does. Polarization-dependent linear and nonlinear optical properties, therefore, depend on the polytype (20). Among many $A^{III}B^{VI}$ layered compounds, GaS is believed to adopt only the β-type, whereas all three polytypes are reported for GaSe. As for InSe, no general agreement has been made about its structure.

The quasi two-dimensionality of $A^{III}B^{VI}$-type layered material raises important questions regarding the origin of its chemical bondings and electronic states. The standard crystal chemical argument of filling of the anion valence subshells in the $A^{III}B^{VI}$ layered compounds would result in an ionic configuration of $III^{2+}VI^{2-}$. In this model the III and VI ions would attract each other and from an ionic bond, whereas the III–III interaction in the middle of each layer would be highly unstable due to coulombic repulsion. Therefore the ionic picture of the chemical bonding fails. The nature of chemical bonding can be partly understood using a simple argument for the covalent interactions in which electrons are transferred to satisfy covalent bonding requirements. In the case of GaSe, one Ga *s*-electron is promoted to the *p*-orbital and one Se *p*-electron is transferred into a cation *p*-level, giving rise to a Ga^{1-},

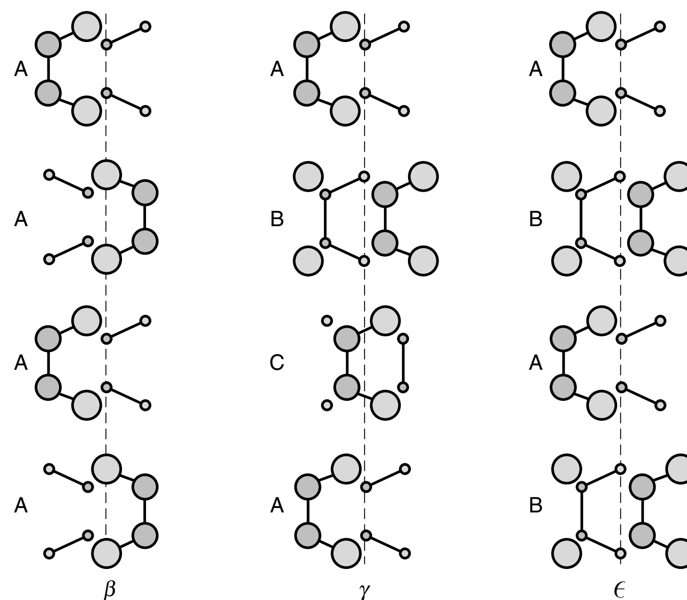

Figure 3. Common polytype stacking for $A^{III}B^{VI}$ materials.

Se^{1+} configuration. This allows Ga to form four covalent bonds with sp^3-type hybridization with adjacent Ga or Se, in which the Ga–Ga bond is likely to be formed predominantly by *s*-electrons whereas the Ga–Se bonds involve more *p*-electrons. The Se *s*-electrons would occupy nonbonding lone-pair orbitals, resulting in no reactive dangling bonds on the layer surfaces. When cleaved along the basal plane, a nearly defect free surface with no exposed dangling bonds can be obtained.

Quantitative band structure calculations can provide a better understanding of the chemical bonding in $A^{III}B^{VI}$. Depeursinge (21) used an empirical pseudopotential method to study the electronic properties of the family of $A^{III}B^{VI}$ layered compounds. The calculated results of the total valence charge densities for β-InSe, β-GaSe, and β-GaS are shown in Fig. 4. The results indicate that the bonding between A^{III} and B^{VI} consists of mixture of ionic and covalent bonds, in which strong localization of valence electrons around the B^{VI} atoms is evident, and the two A^{III} atoms are linked by the *s*-like bonding charge. Decreasing the ionicity from InSe (fractional ionicity of 0.80) to GaS (0.74) and GaSe (0.66), the electronic charges are spread more toward the A^{III} atom, exhibiting a more covalent character in the A^{III}–B^{VI} bond. In addition, the electronic charges between the two A^{III} atoms are more delocalized from InSe to GaSe. When Ga is replaced with In, and Se is replaced with S, the atomic *s*-states of the A^{III} atom become less separated from the B^{VI} *p*-states, leading to the delocalization of the A^{III}–A^{III} bond charge and the weakening of the bond strength (or increasing of the bond length). A crystal like InS becomes unstable, since the atomic In *s*-states are at higher energy than the S *p*-states, and the In–In *s*-like antibonding state lose two electrons transferred to the S p_z-like antibonding states which appear at lower energy. These new charges couple neighboring units in the *z* directions, resulting in the fact that InS is no longer a two-dimensional layered compound but rather crystallizes in a three-dimensional orthorhombic structure.

$A_2^{III}B_3^{VI}$ Compounds

Semiconductors of the type $A_2^{III}B_3^{VI}$ have a "loose" lattice based on wurtzite or zincblende, in which one third of the cationic sites are vacant (22). Among these materials, Ga_2Se_3 and In_2Se_3 have been most widely studied for their potential use as new optoelectonic materials. They crystallize into two forms, α and β; in the α-form the vacancies are disordered throughout the crystal, whereas the β-form has an ordered arrangement of vacancies into a monoclinic structure (23). For example, the structure of β-Ga_2Se_3 is a superstructure, originating from the zincblende-type structure of α-Ga_2Se_3, in which one-third of the cation sites are vacant. The formation of the superstructure results from the ordering of the randomly distributed Ga atoms and "structural vacancies (SV)" on the cation sites of the zincblende lattice. Ghémard et al. (24) used a four-circle diffractometer to determine the structure of β-Ga_2Se_3.

This rather complicated structure of the $A_2^{III}B_3^{VI}$ compounds is generally described in Fig. 5 (25), where the positions of atoms are shown in the superstructure unit cell. The B^{VI} atoms are denoted as VI(X) when the nearest neighbors are two A^{III} and two SVs, and they are denoted as VI(Y) when they are surrounded by three A^{III} and one SV. In this notation, one-third of the anion sites are occupied by VI(X) and two-thirds by VI(Y). In addition, the vacancies (SV) and the VI(X) form continuous, unbranched chains through the crystal, directed toward [001]. The (001) planes of the β-$A_2^{III}B_3^{VI}$ superstructure form hexagonal nets, building up the β-$A_2^{III}B_3^{VI}$ structure by stacking in the sequence VI–III–VI–III. The space group is C_8^4–C_c.

THIN-FILM GROWTH

Most studies of the properties of III–VI semiconductors have been performed on bulk crystals. However, exploitation of

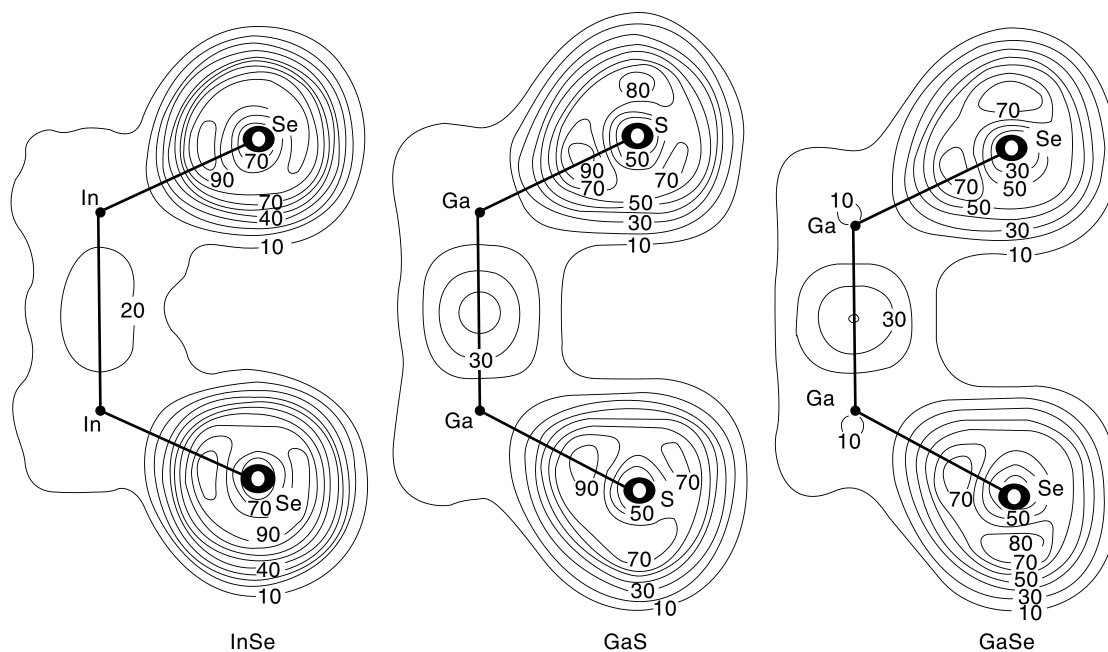

Figure 4. Total valence charge density computed for β-InSe, β-GaSe, and β-GaS (22).

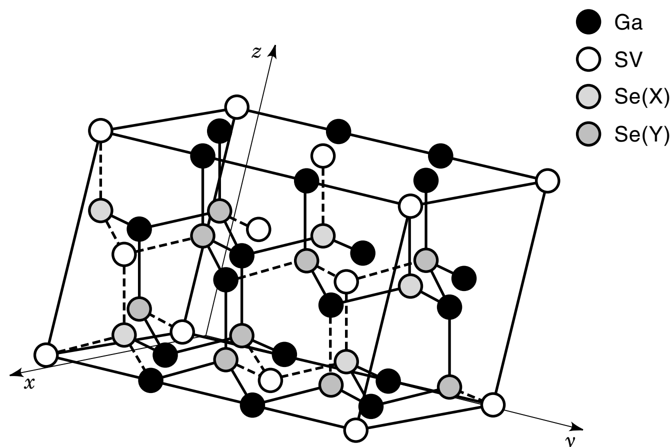

Figure 5. Crystal structure of ordered $A_2^{III}B_3^{VI}$.

these materials for practical applications is hampered by their poor mechanical and thermal properties. Potential use of these materials is therefore largely in thin-film forms, making the growth of III–VI thin films a critical subject. In this section, the recent progress on III–VI thin-film growth is reviewed.

van der Waals Epitaxy

In the layered III–VI semiconductor, the interlayer forces are dominated by interactions between the lone-pair orbitals on the chalcogen atoms. To form a heteroepitaxial film on either a covalent or ionic substrate, it is necessary to create a substrate surface presenting similar nonbonding orbitals to those on the outside of the III–VI layers. The interaction between substrate and film is weak, and this weak bonding removes both the lattice and thermal expansion matching requirements that severely limit material selection in the ordinary heteroepitaxial growth. This mode of the epitaxial growth is called van der Waals epitaxy (VDWE).

There have been an increasing number of reports in the literature on the subject of van der Waals epitaxy since 1985 (26–36). Although the VDWE was originally applied to the heteroepitaxy of a two-dimensional layered chalcogenide overgrown on a different layered chalcogenide (i.e., layered thin film on top of layered materials), more recent applications have focused on the growth of a layered material on more conventional electronic materials, such as Si and GaAs. These substrate materials contain dangling bonds at their surface, and it has been suggested that termination of the surface dangling bonds is a necessary condition for initiating the growth of a van der Waals material. The experimental technique involved in VDWE is essentially the same as molecular beam epitaxy (MBE), with the difference being associated with the interactions between the substrate and the evaporated film. As VDWE is still under development, a typical VDWE growth chamber is equipped with reflection high-energy electron diffraction (RHEED) along with deposition crystal monitor, so that the growth process can be monitored in situ and at real time. To allow for full characterization of the resultant films, the growth chamber may be connected to an analytical chamber, where surface analysis of the thin film can be made.

VDWE of layered III–VI semiconductors may be made by deposition from either two independent molecular beam sources of A^{III} and B^{VI}, a single source of $A^{III}B^{VI}$ compound, or a combination of $A^{III}B^{VI}$ and B^{VI} sources. An advantage of separate sources is the ability to control the group III and group VI fluxes independently, enabling variation of the $B^{VI}A^{/III}$ ratio in the beam equivalent pressure (BEP). A single source, on the other hand, is much simpler to use. A further difference is the nature of the incident species. For GaSe growth, the species are Ga + Se_x for separate sources, where x depends on whether or not the large Se molecules are cracked by a hot filament, and Ga_2Se + Se_2 for sublimation of a GaSe source (37). Stoichiometric GaSe may be obtained using either (a) a stoichiometric GaSe source or (b) a mixture of elemental sources with a BEP ratio $\gg 1$.

The processes of VDWE growth are divided into two primary stages: (1) the heterointerface formation where the interfacial physics and chemistry play decisive roles and (2) the subsequent thin-film growth where homoepitaxial nucleation and growth dominate. In the following sections, GaSe growth on different substrates is highlighted with an emphasis of obtaining a single crystalline GaSe thin film.

GaSe Thin-Film Growth on GaAs(111) Substrates

The epitaxial growth of GaSe on GaAs is a prototypical example of van der Waals epitaxy, exhibiting a 6% lattice mismatch at the heterointerface. Early studies of GaSe growth on untreated GaAs substrates used separate GaSe sources, with an overpressure of Se to facilitate Se termination of the GaAs surface (38). Rumaner et al. (39,40) investigated the nucleation and growth of GaSe on GaAs(111) using a single GaSe source with XPS, RHEED, and AFM techniques. All these data indicated that termination of GaAs dangling bonds by Se occurred prior to the formation of GaSe. In terms of Se bonding to the GaAs surface, there was no evidence for Se–As bonding but rather a Se–As replacement reaction was observed. Subsequent deposition resulted in the formation of rotationally aligned, stoichiometric GaSe layers, overcoming a lattice mismatch in the GaAs(111) A and (111)B cases.

While van der Waals epitaxy is achieved for both substrates, there are significant differences in the growth of the first GaSe molecular layer on GaAs(111)A and (111)B substrates. This indicates the importance of surface structure and stoichiometry in initiating GaSe growth on GaAs. The observed differences include (1) a higher sticking coefficient for Se-containing species on the (111)A surface than on the (111)B, (2) high-binding-energy photoemission components associated with the uncovered, reacted substrate on the (111)B surface that are absent on the (111)A surface at a comparable exposure to the incident flux, (3) a more rapid depletion of As emission on the (111)A surface than on the (111)B surface, and (4) more rapid disappearance of the substrate RHEED patterns on the (111)A surface than on the (111)B.

For the ideal (111)B surface, the top half of the double layer is occupied by As. To first order, the second-layer Ga atoms each contribute an average of 3/4 electron per bond to each of three top layer atoms and the surface As has a partially occupied dangling bond orbital. The stable configuration for either As or Se in the top layer would be three back bonds (contributing an average of 5/4 electron each) to the second-layer Ga plus a fully occupied lone-pair orbital, for a total of

five 3/4 electrons per surface atom. This average is obtained for a $Ga_4Se_3As_1$ surface stoichiometry. For the (111)A surface, Ga occupies the top half of the double layer. Electron counting arguments for this surface show the remaining three Ga atoms per unit cell to have empty surface orbital and no dangling bonds, something which is likely to be true locally even in the absence of long-range order. There is thus no obvious reason for Se to bond or replace As on this surface before growth of stoichiometric GaSe. Calculations for a (1 × 1) structure of monolayer S on GaAs(111)A support a site directly above the Ga atoms (41), which results in a surface that is quite similar electronically to the GaAs(111)B surface.

The photoemission spectra for Ga(3*d*), As(3*d*), and Se(3*d*) regions after 0.5 molecular layers of GaSe on GaAs(111)B and GaAs(111)A surfaces are compared in Figs. 6(a) and 6(b), respectively. Apparent differences are that all the Se, As, and Ga peaks for the case of GaAs(111)B contain small contributions at a binding energy (−1.8 eV relative to the bulk GaAs position), whereas there are no such clear components at higher binding energy for the case of GaAs(111)A, nor have they been observed for exposure of GaAs(111) (42) or GaAs(100) (43–45). These higher-binding-energy components are attributed to the region of the GaAs surface that has partially reacted with the incident flux, but on which bulk GaSe has not yet nucleated.

Further evidence of Se termination was found in the change in band bending during growth of GaSe. Surface dangling bonds behave as electronic defects and act to pin the Fermi level near mid-bandgap in GaAs (42,46). This pinning results in a band banding at the surface of thermally cleaned GaAs(111)B substrate is shown in Fig. 7. For *n*-type GaAs, the pinning of the Fermi level at a location near the midbandgap results in a decrease in the measured GaAs binding energy relative to an unpinned surface [Fig. 7(a)]. The shift of 0.4 eV in the GaAs binding energy in XPS measurement after 0.5 molecular layer GaSe deposition is evidence for the removal of midgap pinning states [Fig. 7(b)]. For the (111)A surface, the reduction in surface band bending does not occur until completion of the first GaSe layer. This is consistent with the S/GaAs(111)A calculations indicating (a) the persistence of midgap states upon addition of a group VI monolayer (40) and (b) a gradual increase in the *n*-type doping of the near surface region through Se–As exchange. The difference in valence band offset in the two cases also implies a different interface dipole.

Schematic diagrams of the GaAs(111)A and GaAs(111)B surfaces and the subsequent growth of GaSe are shown in Fig. 8. The incident flux impinges on the heated GaAs surface. At the (111)B surface, the incident flux reacts with the surface, although both Se stick to Ga. The Se fill As vacancies and complete the surface bilayer, recruiting Ga as needed from the incoming Ga-containing species that initially react with surface aspirates. The surface is likely smoother by these reactions. The data are consistent with the $Se_{0.75}As_{0.25}$ stoichiometry in the surface layer needed to remove states that pin the Fermi level; the removal of these states is confirmed by the shift in the bulk GaAs energy toward flat-band conditions. Once the reactive dangling bonds are removed, a stoichiometry, crystalline GaSe layer nucleates and grows. Deposition of GaSe on the (111)A surfaces immediately initi-

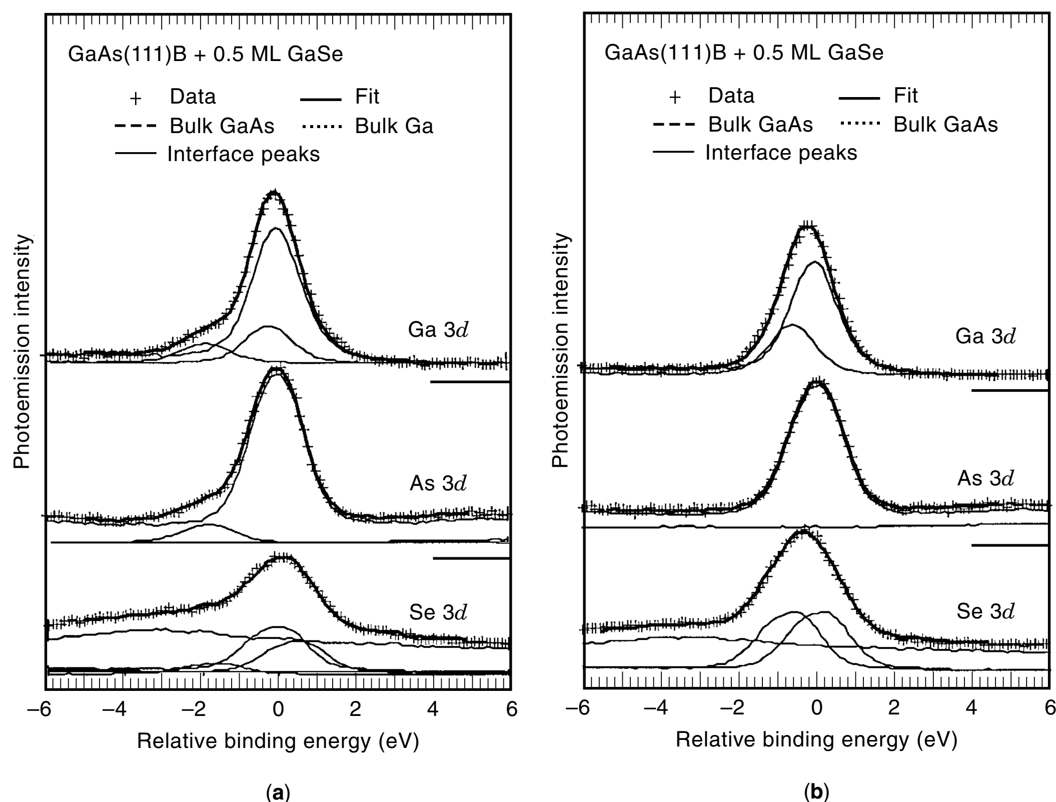

Figure 6. Photoemission spectra for the Ga(3*d*), As(3*d*), and Se(3*d*) regions for 0.5 molecular layer (ML) of GaSe of (a) GaAs (111)B and (b) GaAs(111)A surfaces.

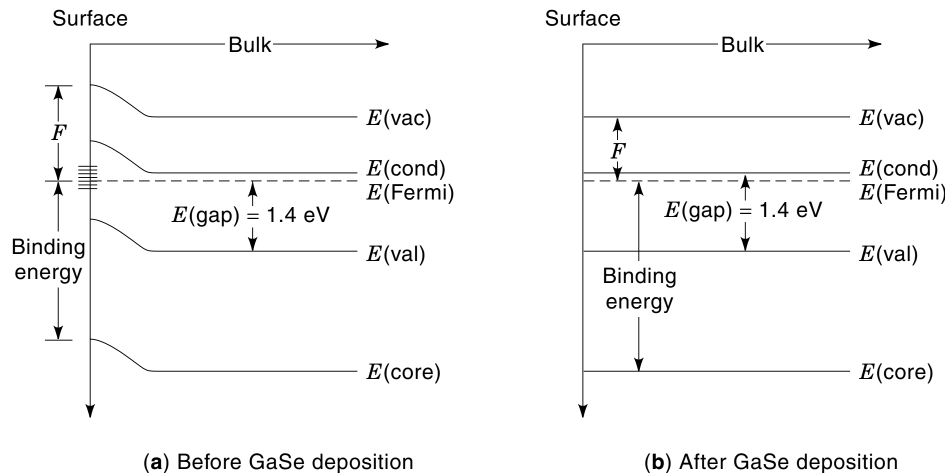

Figure 7. Relationship between the electronic band structure and the measured XPS spectrum. (a) Before GaSe deposition. (b) After GaSe deposition.

ates the surface reaction, with no observed intermediate state.

GaSe Thin-Film Growth on Si (111) Substrates

In bulk silicon, each atom contributes equally to the covalent bonds, so that the termination of the dangling bonds is relatively simple. Replacement of the top Si(111) layer by H leads to fully passivated and unreconstructed Si(111) surfaces. Kuang et al. (47) have used HF treatment of Si(111) to inactive the dangling bonds on which GaSe thin films were grown. H termination was also made through NH_4F treatment, and the growth of GaSe (35) was studied by atomic force microscopy (AFM). While the effectiveness of H-Si(111) has been proven by a number of experiments, H desorbs from Si(111) at around 500°C (48). Since the deposition temperatures are similar, the role of H during the growth is still unresolved. Zheng et al. (36) have recently studied the early stage of growth of GaSe on H terminated Si(111) using x-ray standing wave fluorescence (XSWF). The analysis indicated that Ga atoms were located on the sites directly above the top Si atoms, forming a Si–Ga bond of length 0.237 nm (2.37 Å). This implies that the first step for half of a GaSe layer is to covalently bond to Si at the interface, with van der Waals growth of GaSe layers occurring in a second stage. Although the hydrogen is not visible with XSWF, electron counting arguments lead to the belief that it has been replaced by GaSe at the interface, as opposed to remaining at the interface passivating Si dangling bonds. TEM structural analysis supports this model (49).

An alternate method for passivating the Si(111) substrate is to replace the top Si(111) layer by As. An unreconstructed, passivated surface with As lone-pair states on the surface, very similar to the Se states bounding GaSe layers, is obtained (50,51), promoting high-quality growth of GaSe. One advantage of using As over H is that As does not desorb until over 700 °C and will replace H at the surface under mild annealing (52). Palmer et al. (53) studied the growth of GaSe on As-passivated Si(111) substrate by MBE for a wide range of substrate temperatures (375°C to 500°C) and Se/Ga BEP ratios (30 to >200). A phase diagram for GaSe growth on As:Si(111) was established as shown in Fig. 9. Continuous layered structure GaSe films were formed for high Se/Ga BEP ratios and high substrate temperatures. During the growth, RHEED confirmed that the thin films were flat; however, the surface roughened on a microscopic scale after the growth. Cross-sectional TEM measurements showed atomic scale roughness at the interface after capping the GaSe layer with GaAs (54,55). Similar facetting has been observed for annealed ZnSe/Si(001):As (56), but this was interpreted as the interface rearranging to form lower-energy (111) facets. It is unclear why faceting would occur for the (111)-oriented substrate in this case. At low Se/Ga BEP ratios and high substrate temperatures, only Ga droplets, but no GaSe thin film, formed on the substrate. When either the substrate temperature or the Se/Ga BEP ratio was low, both GaSe thin films and Ga droplets formed simultaneously. Three regimes of growth modes were partly explained in terms of competition between the coarsening of Ga, the formation of GaSe solid phase on Si(111):As, and the formation of volatile Ga_2Se. The outcomes of the competition was determined by the rates of these reactions, which were specific to the substrate temperature and the relative abundance of Ga and Se.

Thin-Film Growth on Cubic Substrates

Use of a cubic substrate, such as (001)GaAs (57,58) or (001)GaP (59), facilitates III–VI thin-film growth in the $A_2^{III}B_3^{VI}$ form under appropriate conditions. The three-dimensional crystal structure of the $A_2^{III}B_3^{VI}$ compounds, unlike the layered $A^{III}B^{VI}$ compounds, means that heteroepitaxial growth of the $A_2^{III}B_3^{VI}$ materials is governed strongly by the substrate lattice spacings and symmetries. As shown in Fig. 1, Ga_2Se_3 and (001)GaP are closely lattice-matched. Using this combination, a single crystalline Ga_2Se_3 thin films with good quality was obtained (61). Ga_2Se_3 layers are also formed during the initial stages of MBE growth of ZnSe on (001) GaAs under As-deficient conditions (60,37). Ga_2Te_3 is another example of the III–VI compounds formation during the early growth stages of ZnTe on (001)GaAs (13,62).

Effects of the Se/Ga BEP and substrate temperature on the thin-film structure and stoichiometry during the growth of Ga–Se thin films on GaP(001) were investigated by Yamada et al. (63). At BEP ratios below 1.0, deposition of Ga_2Se_3 was not observed due to the reevaporation of the Ga and Se components. For the ratios between 1 and 10, the growth rate is now limited by the supply of Se atoms, and the primary phase is GaSe. As the BEP ratio increases further,

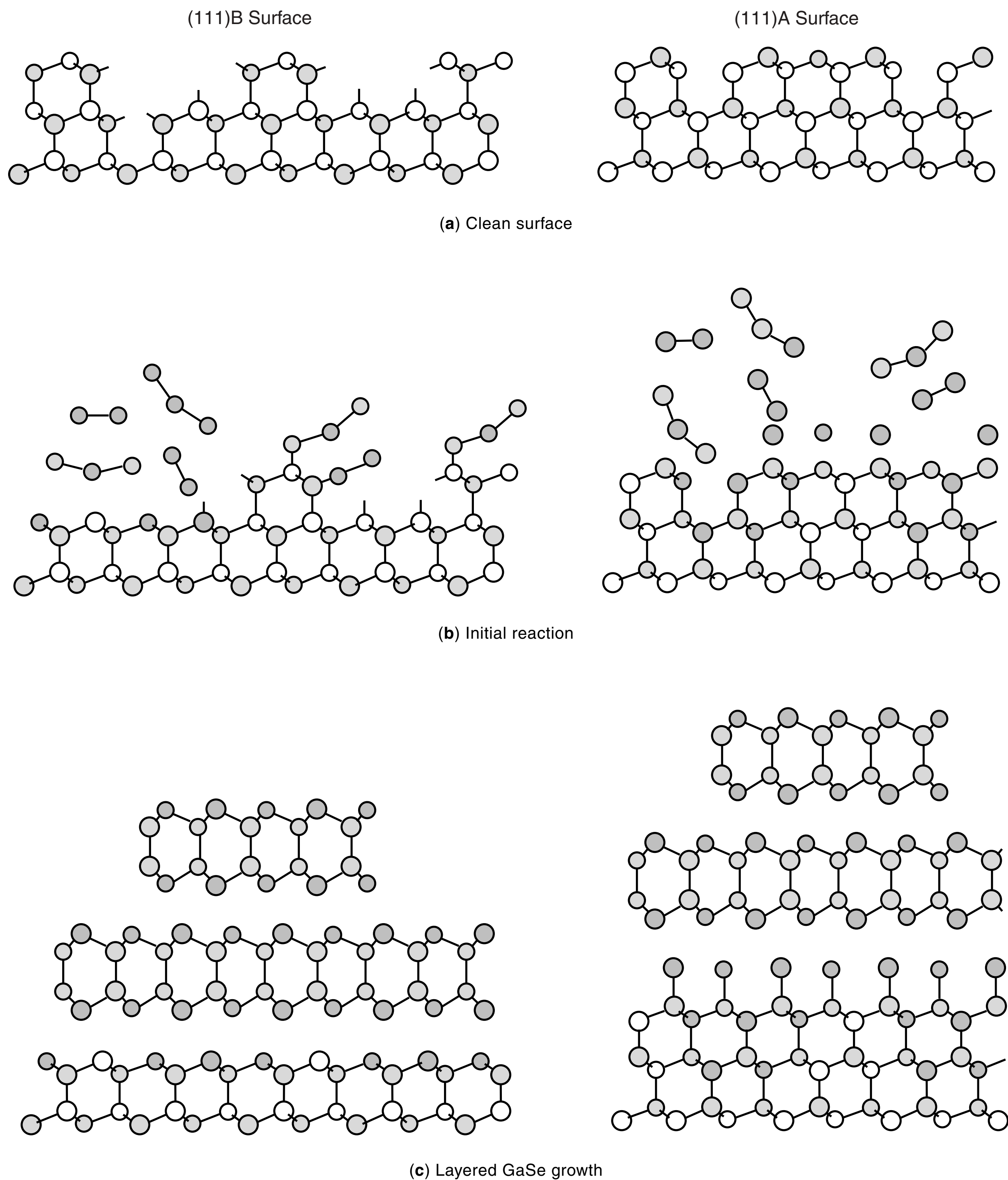

Figure 8. Schematic diagram of the deposition and growth of GaSe on GaAs(111)B and GaAs(111)A surface. (a) Schematic of initial substrate. (b) Reaction of surface with Ga_2Se and Se_2 incident beam. (c) Two layers of GaSe on Se-terminated GaAs(111) surface.

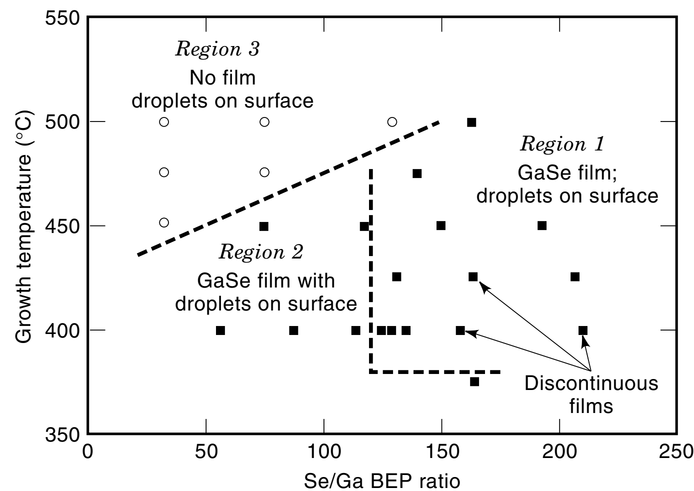

Figure 9. Phase diagram for GaSe growth on As:Si(111).

the growth is determined by the supply of Ga atoms, and the Ga_2Se_3 dominates. In this reaction, a Ga_2Se_3 epitaxial layer is formed in the interface region, which exhibits a highly developed pseudo-two-dimensional ordering of structural vacancies. These vacancies form in a $c(2 \times 2)$ arrangement in the first (100) Ga layer with a shift by $a/2(011)$ with respect to the location of the first Ga layer (a is the unit cell size). Ga_2Se_3 may also be grown by simply exposing GaAs(001) to H_2Se (64). The GaAs surface is initially heated to desorb As and create a Ga-rich condition before the admission of H_2Se. This Ga is then available for reaction with Se to form a compound. Once the GaAs substrate is fully covered, As atoms diffuse from the underlying GaAs through the grown film and out into the gas-phase region of the reactor. The diffusion of As through the Ga_2Se_3 is facilitated by the inherent vacancies present in the film. The presence of As within the grown layer was confirmed by both Raman spectroscopy and secondary ion mass spectrometry, suggesting that the Ga_2Se_3 can be doped to a higher level than order tetrahedral levels of vacancies. In order to balance the charge in the structure, one-third of a Ga atom must be effectively lost for every As replaced by Se. This means that the films "grow" in two directions simultaneously, with Se diffusing through the layer down to the substrate interface and excess Ga diffusing upwards to react with more Se from the vapor phase. The relative position of the internal interface is therefore approximately two-thirds of the total layer thickness from the substrate interface, which was observed by HREM (65). On a rough GaAs(001) substrate, TEM and RHEED measurements revealed both Ga_2Se_3 and GaSe in the same growth; for a smooth starting surface and a stoichiometric GaSe source stream, high flux favors the layered GaSe form while lower flux favors the cubic Ga_2Se_3 form (40). This suggests that terrace nucleation may lead to formation of the more stable $A_{III}B_{VI}$ material, while nucleation at steps and kinks on the surface (favored by low flux) enhances the energetics for forming the cubic phase.

MOCVD Growth

Versatility, high growth rates, and the ability to use a wide range of metal–organic precursors and deposition conditions make metal–organic chemical vapor deposition (MOCVD) a highly desirable route for materials synthesis. MOCVD has recently been adopted to grow Ga_2Se_3 thin films on nearly lattice-matched GaP and lattice-mismatched GaAs substrates (66). Although pre-reacting trimethylgallium (TMGa) with the hydride H_2Se in the gas phase has yielded thin films which are only partially expitaxial, the combination of TMGa with ditertiary-butylselenide produces thin films with relatively good quality under steady state flow conditions. Ng et al. also reported GaAs was not a suitable substrate for MOCVD growth due to exchange reactions at the interface leading to poorly bonded thin films (66). Although fundamental thermodynamic and kinetic data on the chemical precursors used in III–VI formation are largely lacking, Maung et al. (67) have recently conducted a mass-spectrometric study of the pyrolysis reactions using TMGa and H_2Se, suggesting that the gas-phase adducts are significant intermediates, followed by irreversible deposition of the polymeric adduct of Ga_2Se_3 on the substrate.

A single-source precursor in MOCVD has its own advantage for simplicity. Schulz et al. (68) have recently developed new molecules called gallium-chalcogen heterocubanes $[Cp^*Ga(\mu_3\text{-}E)]_4$, where E = S and Se. One attractive feature of cubanes as single-source precursors for MOCVD reactions are their clean decomposition pathways. They have demonstrated the deposition of Ga_2S_3 and Ga_2Se_3 thin films at 290°C to 310°C. While As-deposited films were amorphous, the films crystallized to thermodynamically stable phases upon annealing to 500°C. This development enables gallium sulfide and/or selenide films to be deposited on a wider variety of thermally sensitive substrates.

PROPERTIES OF III–VI MATERIALS AND THIN FILMS TOWARD DEVICE APPLICATIONS

The primary device applications proposed for thin film III–VI materials are buffer layers in heteroepitaxy and polarization-dependent optical materials. The cubic $A_2^{III}B_3^{VI}$ compounds are often unavoidable as thin layers at III–V/II–VI heterointerfaces; it is unknown whether this may be exploited for optimizing device properties. The layered $A^{III}B^{VI}$ materials show definite promise as buffer layers for the relief of lattice and thermal mismatch constraints. The weak VDW bonding between the layers allows a change in lattice constant parallel to the growth direction without the creation of electronically active dislocations or other defects. The XSWF measurements described above showing covalent capping of Si with GaSe and subsequent GaSe layered growth, combined with Gray et al.'s (69) and Palmer et al.'s (70) observation of high-quality GaAs growth on GaSe, demonstrate the possibility of GaSe as a buffer layer promoting GaAs growth on Si(111).

Layered $A^{III}B^{VI}$ materials have received much attention for their large nonlinear optical coefficients (71). The strong polarization anisotropy in linear absorption may also be useful as a polarizer, while the large index of refraction anisotropy may be useful for polarization rotators. The effect is largest if the light propagates parallel to the layers, which leads to difficult alignment problems for bulk crystals. However, heteroepitaxial techniques make it possible to incorporate GaSe layers directly into GaAs optoelectronic structures.

Previous attention has focused on the optical properties of bulk samples. However, thin films enable use in absorbing

spectral ranges, decrease the importance of phase matching, and may be integrated into larger device structures. The polarization-dependent linear and nonlinear optical properties of $A^{III}B^{VI}$ show distinct promise for optical device structures. GaSe and InSe exhibit a large second-order susceptibility $d'(2\omega, \omega, \omega)/\epsilon_0$, $\sim 9 \times 10^{-11}$ m/V and $\sim 19 \times 10^{-11}$ m/V at $\lambda = 1.06$ μm (72), which are similar to the values observed in GaP (73). This allows for frequency conversion over a wide region of the infrared spectrum. It has been demonstrated that GaSe was used as a frequency doubler for the output of a high-power, short-pulse, mid-infrared free-electron laser (74). Internal conversion efficiencies up to 36% were achieved in the wavelength range from 6.3 μm to 12 μm. The second-harmonic output was stable over many hours at peak power levels of 1 MW to 2 MW.

It has recently been shown that the second harmonic generation (SHG) at 1.064 μm reflected by epitaxially grown GaSe thin films on Si(111) was comparable so that generated from the bulk GaSe (75). This suggests the possibility of SHG devices comprising of a multilayer thin film structure. A particular advantage is that they do not require phase matching. The reflected second harmonic signals from thin-film GaSe has been shown as a diagnostic tool for the investigation of orientational order of the layers—in particular, the existence of antiphase domains. X-ray and electron diffraction techniques are not sensitive to the point inversion, making them inappropriate for observing antiphase domains.

In addition to second harmonic generation, phase-matched optical parametric generation in the range $\lambda = 3.5$ μm to 14 μm has been also demonstrated with a 2.9 μm pump laser (76). A resonant enhancement in the fundamental was for the bandgap exciton in GaSe at an energy very close to that of He–Ne radiation (77); using that resonance in the second harmonic may enable efficient up-conversion to the visible of a 1.25 μm diode laser. Alloying GaSe with In or S will move the resonance to other frequencies.

The optical properties of the $A_2^{III}B_3^{VI}$ compounds are intimately connected to the cation vacancies and their ordering. Ga_2Se_3 thin film epitaxially grown on (100)GaP has the vacancy-ordered superstructure, in which the vacancies were predominantly formed in the [011] direction. In the transmission measurements, Okatmoto et al. (78) found a large difference in the absorption coefficients between the lights polarized parallel and perpendicular to the vacancy-ordering directions, and the difference was more than 10^4 cm^{-1} at the wavelength of 525 nm. The vacancy-ordered Ga_2Se_3, therefore, behaves like a polarizer in the selected wavelength. In addition, the vacancy-ordered Ga_2Se_3 thin film exhibits strong anisotropy in photoluminescence (PL) (79); the PL intensity of the $[0\bar{1}1]$ polarization component (perpendicular to the vacancy) is much stronger than that of [011] polarization (parallel to the vacancy). It was also observed that the anisotropy in PL emission was independent to the polarization of the excitation, indicating that the electron transition probability for the $[0\bar{1}1]$ polarization is much larger than that for the [011] polarization.

SUMMARY

Materials based on III–VI compounds have many distinct structural, electronic, and optical properties not found in the more traditional group IV, III–V or II–VI based materials. The III–VI materials comprises two principal classes: (1) layered materials in the form of $A^{III}B^{VI}$ and (2) cubic materials in the form of $A_2^{III}B_3^{VI}$, both of which are of interest as possible novel materials for electronic or optoelectronic devices. The III–VI materials are, however, difficult to work with in bulk form due to their poor mechanical and thermal properties; these problems can be overcome through using thin films. Thin-film growth of these materials are, therefore, important particularly by combining with common electronic materials through heterointerface technology, from which a new regime of material systems may be opened for future development. Present paper has reviewed the III–VI materials from these perspectives.

ACKNOWLEDGMENT

The authors acknowledge many useful discussions with Professor Koma and Dr. Ueno of University of Tokyo and with Dr. L. E. Rumaner and Ms. J. L. Gray of Intel Corporation. Funding for this project was made possible by a grant from the National Science Foundation (NSF #92-09652) and by the New Energy and Industrial Technology Development Organization (NEDO).

BIBLIOGRAPHY

1. F. Hulliger, Structural chemistry of layer-type phases. In R. Levy (ed.), *Physics and Chemistry of Materials with Layered Structure,* Vol. 5, Dordrecht, Holland: Reidel, 1976.
2. J. Dieleman and A. R. C. Engelfriet, The phase diagram of the system $Ga_{1-x}Se_x$ for $0.5 \le x \le 0.6$ and $300\ K < T < 1500\ K$, *J. Less-Common Met.,* **25**: 231–233, 1971.
3. R. LeToullec et al., Optical constants of ϵ-GaSe, *Nuovo Cimento,* **38B**: 159–167, 1977.
4. R. Minder, G. Ottaviani, and N. C. Canali, Charge transport in layered semiconductors, *J. Phys. Chem. Solids,* **37**: 417–423, 1976.
5. G. A. Akhundov et al., Second-harmonic generation in III–VI compounds, *Sov. Phys. Semicond.,* **7**: 826–827, 1973.
6. I. M. Catalan et al., Second-harmonic generation in layered compounds, *Opt. Commun.,* **24**: 105–108, 1978.
7. I. M. Caatalono et al., Second harmonic generation in InSe, *Solid State Commun.,* **30**: 585–588, 1979.
8. N. C. Fernelius, Properties of gallium selenide single crystal, *Prog. Cryst. Growth Charact. Mater.,* **28**: 275–353, 1994.
9. E. E. Ovechkina, V. P. Romanov, and Yu. R. Zabrodskii, “Compression” of the electron shell of a neutral atom by a crystal matrix, *Sov. Phys. JETP,* **45**: 174–178, 1977.
10. V. M. Koshikin, Yu. N. Dmitriedv, and Yu. R. Zabrodskii, Anomalous radiation stability of loose crystal structures, *Sov. Phys. Semicond.,* **18**: 860–863, 1984.
11. A. Krost, A. Richter, and D. R. T. Zahn, Chemical reaction at the ZnSe/GaAs interface detected by Raman spectroscopy, *Appl. Phys. Lett.,* **57**: 1981–1982, 1990.
12. D. R. J. Menke et al., An x-ray photoelectron spectroscopy study of bonding at II–VI/III–V heterovalent interfaces, *J. Vac. Sci. Technol.,* **B9**: 2171–2175, 1991.
13. A. C. Wright and J. O. Williams, Detection of compound formation at the ZnSe/GaAs interface using high resolution transmission electron microscopy (HREM), *J. Cryst. Growth,* **114** (1–2): 99–106, 1991.

14. B. I. Sysoev et al., Insulating coating for gallium arsenide, *Sov. Phys. Technol.,* **31**: 554–555, 1986.

15. S. Takatani et al., Evidence of Ga2Se3-related compounds on Se-stabilized GaAs surfaces, *Jpn. J. Appl. Phys.,* **31** (4B): L458–L460, 1992.

16. N. Teraguchi et al., Growth of III–VI compound semiconductors by metalorganic molecular beam epitaxy, *Jpn. J. Appl. Phys.,* **28**: L2134–L2136, 1989.

17. T. Okamoto et al., Anomalous anisotropy in the absorption coefficient of vacancy-ordered Ga_2Se_3, *J. Electron. Mater.,* **22** (2): 229–232, 1993.

18. A. T. Nagat et al., Anisotropy of electrical conductivity and Hall effect in gallium selenide crystals, *Indian J. Pure Appl. Phys.,* **28**: 586–589, 1990; K. H. Park, W. S. Lee, and W. T. Kim, Electrical properties of Ga_2Se_3:Co single crystals, *New Phys. (Korean Phys. Soc.),* **27** (6):638–641, 1987.

19. A. Gouskov, J. Camassel, and L. Gouskov, Growth and characterization of III–VI layered crystals like GaSe, GaTe, InSe, $GaSe_{1-x}Te$, and $Ga_xIn_{1-x}Se$, *Prog. Cryst. Growth Charact. Mater.,* **5**: 323–413.

20. M. Schlüter et al., Optical properties of GaSe and GaS_xSe_{1-x} mixed crystals, *Phys. Rev.,* **13B**: 3534–3547, 1976.

21. Y. Depeursinge, Electronic properties of the layer III–VI semiconductors: A comparative study, *Nuovo Cimento,* **64B** (1): 111–150, 1981.

22. L. A. Atroshchenko et al., Stoichiometric deviations and solutions of impurities in semiconductor compounds of the $B^{III}{}_2C^{VI}{}_3$ type, *Inorg. Mater.,* **1**: 1935–1943, 1965.

23. D. Lubbers and J. Leute, The crystal structure of β-Ga_2Se_3, *J. Solid State Chem.,* **43**: 339–345, 1982.

24. P. G. Ghémard et al., Structure de la Phase Ordonnée du Sesquiséléniure de Gallium, Ga_2Se_3, *Acta Crystallogr.* **C39**: 968–971, 1983.

25. P. C. Newman, Ordering in $A^{III}{}_2B^{VI}{}_3$ compounds, *J. Phys. Chem. Solids,* **23**: 19–23, 1962; P. C. Newman, Crystal structure of adamantine compounds, *J. Phys. Chem. Solids,* **24**: 45–50, 1962.

26. A. Koma, K. Sunouchi, and T. Miyajima, Fabrication of ultrathin heterostructures with van der Waals epitaxy, *J. Vac. Sci. Technol.,* **3** (2): 724, 1985.

27. A. Koma and K. Yashimura, Ultrasharp interfaces grown with van der Waals epitaxy, *Surf. Sci.,* **174** (1–3): 556–560, 1986.

28. A. Koma, K. Saiki, and Y. Sato, Heteroepitaxy of a two-dimensional material on a three-dimensional material, *Appl. Surf. Sci.,* **41–42**: 451–456, 1989.

29. F. S. Ohuchi et al., Van der Waals epitaxial growth and characterization of $MoSe_2$ thin films on Sns_2, *J. Appl. Phys.,* **68**: 2168–2175, 1990.

30. F. S. Ohuchi et al., Growth of $MoSe_2$ thin films with van der Waals epitaxy, *J. Cryst. Growth,* **111** (1–4): 1033–1037, 1991.

31. H. J. Osten, J. Klatt, and G. Lippert, Van der Waals epitaxy of thick Sb, Ge and Ge/Sb films on mica, *Appl. Phys. Lett.,* **60**: 44–46, 1992.

32. R. Schlaf et al., Van der Waals epitaxy of thin InSe films on $MoTe_2$, *Surf. Sci.,* **303** (1–2): L343–L347, 1994.

33. K. Ueno, M. Sakurai, and A. Koma, Van der Waals epitaxy on hydrogen terminated Si(111) surfaces and investigation of its growth mechanism by atomic force microscope, *J. Cryst. Growth,* **150** (1–4): Part 2, 1180–1185, 1995.

34. T. Loher et al., Van der Waals epitaxy of three-dimensional CdS on two-dimensional layered substrate $MoTe_2$(0001), *Appl. Phys. Lett.,* **65**: 555–557, 1994.

35. K. Ueno, M. Sakurai, and A. Koma, Van der Waals epitaxy on hydrogen-terminated Si(111) surfaces and investigation of its growth mechanism by atomic force microscope, *J. Cryst. Growth,* **150** (1–4): Part 2, 1180–1185, 1995.

36. Y. Zheng et al., GaSe/Si(111) heteroepitaxy: The early stages of growth, *J. Cryst. Growth,* **162** (3–4): 135–141, 1996.

37. A. Ludniksson et al., Vacuum sublimation of GaSe; a molecular source for deposition of GaSe, *J. Cryst. Growth,* **151** (1–2): 114–120, 1995.

38. K. Ueno et al., Heteroepitaxy of layered semiconductor GaSe on a GaAs(111)B surface, *Jpn. J. Appl. Phys.,* Part 2, **30** (8): L1352–L1354, 1991.

39. L. E. Rumaner, *Nucleation and growth in van der Waals epitaxy,* Ph.D. thesis, University of Washington, Seattle, WA, 1995.

40. L. E. Rumaner et al., Substrate effects on the nucleation and growth of GaSe layers by van der Waals epitaxy, *Structure and Properties of Multilayered Thin Films,* Materials Research Society Symposium, San Francisco, CA, 1995, pp. 101–106.

41. T. Ohno, Sulfur passivation of GaAs surfaces, *Phys. Rev.,* **B44**: 6306–6311, 1991.

42. T. Scimeca et al., Surface chemical bonding of selenium-treated GaAs(111)A, (100), and (111)B, *Phys. Rev.,* **B46**: 10201–10206, 1992.

43. S. A. Chambers and V. S. Sundaram, Structure, chemistry, and band bending at Se-passivated GaAs(001) surfaces, *Appl. Phys. Lett.,* **57**: 2442–2344, 1990; *ibid.*, Passivation of GaAs(001) surfaces by incorporation of group VI atoms: A structural investigation, *J. Vac. Sci. Technol.,* **B9**: 2256–2262, 1991.

44. S. Takatani, T. Kikawa, and N. Nakazawa, Reflection high-energy electron-diffraction ad photoemission spectroscopy study of GaAs(001) surface modified by Se adsorption, *Phys. Rev.,* **B45**: 8498–8505, 1992.

45. F. Maeda et al., Surface structure of Se-treated GaAs(001) from angle-resolved analysis of core-level photoelectron spectra, *Phys. Rev.,* **B48**: 4956–4959, 1993.

46. J. Szuber, The influence of oxygen adsorption on the electronic surface states and the Fermi level pinning on the clean, polar GaAs(111) surface, *Appl. Surf. Sci.,* **55**: 143–147, 1992.

47. Y. L. Kuang et al., Heteroepitaxial growth of layered semiconductor GaSe on a hydrogen-terminated Si(111) surface, *Jpn. J. Appl. Phys.,* Part 2 **32** (3B): L434–L437, 1993.

48. B. G. Koehler et al., Desorption kinetics of hydrogen and deuterium from Si(111) 7×7 studied using laser-induced thermal desorption, *J. Chem. Phys.,* **89**: 1709–1718, 1988.

49. A. Koebel et al., A transmission electron microscopy structural analysis of GaSe thin films grown on Si(111) substrates, J. Cryst. Growth, **154** (3–4): 269–274, 1995.

50. M. A. Olmstead et al., Arsenic overlayer on Si(111): Removal of surface reconstruction, *Phys. Rev.,* **B34**: 6401–6044, 1986.

51. R. I. G. Uhrberg et al., Electronic structure, atomic structure and the passivated nature of the arsenic-terminated Si(111) surface, *Phys. Rev.,* **B35**: 3945–3951, 1987.

52. R. D. Bringans and M. A. Olmstead, The bonding of arsenic to the hydrogen terminated Si(111) surface, *J. Vac. Sci. Technol.,* **B6**: 1132–1136, 1988.

53. J. E. Palmer et al., Growth of GaSe on As-passivated Si(111) substrates, *J. Cryst. Growth,* **147**: 283–291, 1995.

54. J. E. Palmer et al., Growth and characterization of GaSe and GaAs/GaSe on As-passivated Si(111) substrates, *J. Appl. Phys.,* **74**: 7211–7222, 1993.

55. J. E. Palmer et al., Growth and characterization of GaAs/GaSe/Si heterostructure, *Jpn. J. Appl. Phys.,* Part 2, **32**: L1126–L1129, 1993.

56. R. D. Bringans et al., Effect of interface chemistry on the growth of ZnSe on the Si(100) surface, *Phys. Rev.,* **B45**: 13400–13406, 1992.

57. Y. Nakamura, Ordering of structural vacancies at Ga_2Se_3/GaAs epitaxial interface, *J. Crystallograph. Soc. Jpn.,* **34** (4): 255–259, 1992.
58. A. C. Wright et al., High resolution and conventional transmission electron microscopy of Ga_2Se_3 thin films grown by vapor phase epitaxy, *J. Cryst. Growth,* **121**: 111–120, 1992.
59. N. Teraguch et al., Growth and characterization of Ga_2Se_3 by molecular beam epitaxy, *J. Cryst. Growth,* **115**: 798–801, 1991; N. Teraguch, M. Konagai, F. Kato, and K. Takahashi, Vacancy ordering of Ga_2Se_3 films by molecular beam epitaxy, *Appl. Phys. Lett.,* **59**: 567–569, 1991.
60. J. Qiu et al., Characterization of Ga_2Se_3 at ZnSe/GaAs heterovalent interfaces, *Appl. Phys. Lett.,* **58**: 2788–2790, 1991.
61. D. Li et al., Vacancy ordering at heterovalent interface, *Surf. Sci.,* **267** (1–3): 181–186, 1992.
62. J. O. Williams, A. C. Wright, and H. M. Yate, High resolution and conventional transmission electron microscopy in the characterization of thin films and interfaces involving II–VI materials, *J. Cryst. Growth,* **117** (1–4): 441–453, 1992.
63. A. Yamada and M. Konagai, Vacancy-ordered Ga_2Se_3 and its optical anisotropy, *Ohyo Butsuri,* **63** (20): 165–168, 1994 (in Japanese).
64. D. R. T. Zhan et al., Epitaxial Ga_2Se_3 layers grown on GaAs(100) using a heterovalent exchange reaction. *J. Vac. Sci. Technol.,* **B** (10): 2077–2081, 1992.
65. A. C. Wright et al., High resolution and conventional transmission electron microscopy of Ga_2Se_3 thin films grown by vapor phase epitaxy, *J. Cryst. Growth,* **121**: 111–120, 1992.
66. T. L. Ng et al., Metal–organic vapor phase epitaxial growth of cubic gallium selenide, Ga_2Se_3, *Chem. Vap. Deposition,* **2** (5): 185–189, 1996.
67. N. Maung et al., Mass-spectrometric study of the pyrolysis reactions in the MOVPE of Ga_2Se_3 by in-situ gas sampling, *J. Cryst. Growth,* **158**: 68–78, 1996.
68. S. Schulz et al., Synthesis of gallium chalcoenide cubanes and their use as CVD precursors for Ga_2E_3 (E = S, Se), *Organometallics,* **15**: 4880–4883, 1996.
69. J. L. Gray et al., Van der Waals epitaxy versus homoepitaxy of low temperature GaAs (111) layers, Proceedings of the Materials Research Society, *Compound Semicond. Epitaxy,* **340**: 381–385, 1994.
70. J. E. Palmer et al., GaAs on Si(111) with a layered structure GaSe buffer layer, *J. Cryst. Growth,* **150** (1–4): 685–190, 1995.
71. G. C. Bhar, S. Das, and K. L. Vodopyanov, Nonlinear optical laser devices using GaSe, *Appl. Phys. B,* **B61** (2): 187–190, 1995.
72. E. Bringuier et al., Optical second-harmonic generation in lossy media: Application to GaSe and InSe, *Phys. Rev.,* **B49**: 16971–16982, 1994.
73. B. F. Levine and C. G. Bethea, Nonlinear susceptibility of GaO; relative measurement and use of measured values to determine a better absolute value, *Appl. Phys. Lett.,* **20**: 272–235, 1972.
74. J. M. Auerhammer and E. R. Eliel, Frequency doubling of mid-infrared radiation in gallium selenide, *Opt. Lett.,* **21**: 773–775, 1996.
75. J. Amzallag et al., Second harmonic generation as a probe of antiphase domains in layered GaSe thin films on Si(111) substrates, *Appl. Phys. Lett.,* **66**: 982–984, 1995.
76. K. L. Vodopyanov and L. A. Kulevskii, New dispersion relationships for GaSe in the 0.65–18 μm spectral region, *Opt. Commun.,* **118**: 375–378, 1995.
77. C. Hirlimann, J.-F. Morhange, and A. Chevy, Excitonic resonant second harmonic in GaSe, *Solid State Commun.,* **69**: 1019–1022, 1989.
78. T. Okamoto et al., Optical anisotropy of vacancy-ordered Ga_2Se_3 grown by molecular beam epitaxy, *Jpn. J. Appl. Phys.* (Part 2), **31** (2B): L144–L144, 1992.
79. T. Okamoto et al., Polarized photoluminescence in vacancy-ordered Ga_2Se_3, *J. Cryst. Growth,* **138**: 204–207, 1994.
80. H. Landolt and R. Bornstein, Numerical data and functional relationships in science and technology. In *Landolt–Börnstein Physikalisch-chemische Tabellen,* Berlin: Springer Verlag, 1961–1995.

F. S. Ohuchi
M. A. Olmstead
University of Washington